Evidence of iso-volume deformation during convective drying of yacón: An extended van Meel model adapted to large volume reduction

Bianca Marques, Patrick Perré, Joel Casalinho, Carmen Tadini, Artemio Plana-Fattori, Giana Almeida

Evidence of iso-volume deformation during convective drying of yacón: an extended van Meel model adapted to large volume reduction.

Bianca Marques[a], Patrick Perré[b,c], Joel Casalinho[c], Carmen C. Tadini[a,d], Artemio Plana-Fattori[e], Giana Almeida[e,*]

[a]*Universidade de São Paulo, Escola Politécnica, Dept. of Chemical Engineering, Main Campus, São Paulo, Brazil*
[b]*Université Paris-Saclay, CentraleSupélec, LGPM, Centre Européen de Biotechnologie et de Bioéconomie (CEBB), 3 rue des Rouges Terres, 51 110 Pomacle, France*
[c]*Université Paris-Saclay, CentraleSupélec, LGPM, 8-10 rue Joliot-Curie, 91 190 Gif-sur-Yvette, France*
[d]*FoRC/NAPAN Food Research Center - Universidade de São Paulo*
[e]*Université Paris-Saclay, INRAE, AgroParisTech, UMR SayFood, 91120, Palaiseau, France*

Abstract

This work investigates the drying of yacón (*Smallanthus sonchifolius*), a source of fructooligosaccharides and inulin, two prebiotic compounds. Experiments were performed using an in-house device consisting of a magnetic suspension balance coupled to a drying chamber and an *in-situ* shadowgraphy system. This allowed the continuous acquisition of mass, sample volume and exhange surface area to be register versus time at different temperatures (50-70°C) and relative humidities (10-30 %), which was never done with yacón. Once corrected by the actual area of the exchange surface, the drying kinetics ($kg.s^{-1}.m^{-2}$) depicts two phases, a very long constant drying rate flux and a falling drying rate flux. Even though yacón samples lost up to 91 % of their initial volume, an iso-volume deformation was observed: the reduction of sample volume equals the volume of removed water. Thanks to these two experimental facts, an extended, original, van Meel model is proposed to account for this huge change of sample shape in a predictive way.

Keywords: Biological product, Cell collapse, Constant Drying Rate, Digital Image Correlation, Exchange surface, Vegetable

1. Introduction

Yacón (*Smallanthus sonchifolius*) is a perennial plant from the Andean region. Most of its varieties are originally from Peru, but some are some found in Bolivia, Ecuador, and neighbouring countries. Its cultivation has recently spread to other countries and continents [20]. The roots are mildly sweet and edible when raw, due to the almost complete absence of starch. Its energy reserves are largely in the form of fructooligosaccharides (FOS) and inulin [21, 44].

The human gastrointestinal tract cannot digest FOS and inulin, because it lacks the necessary enzymes [13]. This leads to two main implications: firstly, yacón roots do not cause a glycemic peak, thus being a sweet alternative for diets with sugar restrictions, such as for diabetics [37]. Secondly, these compounds reach the intestinal microbiota practically intact, leading to prebiotic and immunomodulatory effects [13, 46, 14].

*Corresponding author
Email address: giana.almeida@agroparistech.fr (Giana Almeida)

Yacón roots have a very high moisture content (X), usually higher than 90g /100g fresh weight (dry-basis initial moisture content over 1,000g/ 100g!). The compounds of interest represent about half of the dry content in yacón [21]. The water activity is also high, leading to a short shelf life [34] . A simple but effective way to preserve yacón is to dry the roots before storage, to reduce their water activity. Several studies were carried out to evaluate different aspects of yacón drying, since the drying and blanching processes can lead to a loss of the FOS and inulin, either by lixiviation or hydrolysis [38]. Bernstein and Noreña [6] performed the convective drying of yacón slices, to evaluate the thermophysical properties and volumetric shrinkage along the process. Perussello et al. [33] used an osmo-convective process to dehydrate yacón and estimate the density and the thermal properties of the samples. Scher et al. [38] used a vacuum-aided drying process to dry yacón samples under different temperatures and pretreatment conditions, to verify a possible degradation of the FOS during these processes. Shi et al. [40] used a convective dryer assisted by microwave heating to dry yacón under a range of different conditions, looking for an optimal response in terms of drying rate, color, shrinkage, and rehydration capacity.

However, to our knowledge, the convective drying of the yacón roots under controlled relative humidity was only performed on a pilot scale [23]. Controlling this parameter is a common practice in drying experiments and has been reported for other crops, such as potatoes [19, 2] and apples [4].

In the case of fruits and vegetables, the product usually depict large deformations (shrinkage) during drying. Gorling [16] was one of the first author to account for deformation (the change of thickness) to analyze the drying rate. In this work, thickness was just measured manually using a caliper. Lozano et al. [22] emphasized the effect of shrinkage on porosity in the case of deformable products. As a direct effect of deformation, a rigorous analysis of the drying behavior required the drying rate (time-derivative of mass loss), to be corrected by the actual exchange surface area. The first attempts to follow size and volume used manual measurements at discrete times during the process, removing the sample from the oven [36]. However, *in-situ* and continuous measurements are required to correct the drying rate by the actual surface area. Such an analysis allowed an apparent falling drying rate period to be turned into a constant drying rate flux [24]. This was consistently confirmed by a computational model accounting for the coupling between mechanics and transfers [28]. This constant drying rate flux is usually very long for bio-

logical product. By measuring the surface temperature of the sample, it was proved that this constant drying flux period consistently correspond to a real first drying period, during which the sample remains at the wet bulb temperature [29].

This fact emphasizes the need to measure the sample shape without any perturbation during drying. To obtain accurate measurements, several features should be fulfilled simultaneously : i) continuous measurements (high frequency) of mass and dimensions to follow the time-evolution of shape and drying rate ii) contactless determination to avoid articfacts in deformation iii) *in-situ* measurements to maintain the drying conditions. Several devices have been imagined for that purpose: scanning laser micrometers to follow two dimensions of a simple geometry[24, 29], 2D imaging with suitable image processing [2]. Note that 2D image processing requires further assumptions/constrains to obtain the volume and surface area of the sample. For example, such as in the present work, using axi-symmetrical samples and assuming the sample to keep this shape during drying. Recently, Singh and Talukdar [42] proposed the combination of two images, taken at 90°, to gain a more complete information of the sample shape. Still, the simultaneous interpretation of both images still needs assumptions. In this sense, modern 3D imaging tools such as micro-tomography seems ideal in terms of sample geometry description. However, the scanning time and the difficulty to get *in-situ* measurements are still important concerns. As example of 3D imaging, [6] used a 3D laser scanner to follow the shape of yacón samples during drying. However, the measurements were neither *in-situ* nor continuous and the analyzed results are sparse and quite noisy.

The present work proposes an original study of convective drying of yacón under a range of controlled conditions, using an experimental device especially designed for the continuous measurement of mass and dimensions of samples. The precise control of drying conditions, the accurate measurement of the mass, together with the *in-situ* measurement of sample volume and surface area allow us to obtain novel data regarding the physical behavior of yacón during drying. The experimental device fulfill all conditions for an optimal analysis of the drying behavior, as listed above: i) continuous, ii) contactless iii) *in-situ*. We just assumed and checked that the cylindrical samples remained cylindrical during most of the drying process. To the best of our knowledge, this is the first time all these conditions are met ti study the drying of yacón.

This unique set of experimental data allowed us to prove that yacón depicts a very long first drying period and undergoes an iso-volume deformation during most of the drying

process. These two novelties allows us to propose an extended van Meel model able to account for the huge deformation of the product in a predictive way.

2. Material and Methods

2.1. Material

Yacón root samples (*Smallanthus sonchifolius*) were acquired from a local market, in two 4-kg lots. They were grown in Bretagne, France, and the lots were harvested in January and February 2021. Upon reception, each root was individually wrapped in absorbent paper and PVC film, and kept refrigerated at 4 °C until use, for up to one month. Although the variety was not identified, the roots had a dark-brown peel and a light-yellow flesh. To determine the sorption isotherms, a yacón root was cut into cylinders, 1 cm diameter and approximately 1 mm height, using a cylindrical cheese cutter and a razor blade. As the shrinkage anisotropy is an important information in this work, all samples were cut along well-identified product directions. They were cut from the central axis of the roots, in the longitudinal direction, as shown in Fig. 1a. For the drying experiments, the roots were cut into cylinders with 1.0 cm diameter and 1.2 cm height. Samples were prepared immediately before the tests, to prevent dehydration; and previously blanched in 20 mL of a citric acid solution of 2 g/L, for 3 min.

2.2. Water vapor isotherms

The water vapor sorption isotherms were performed in duplicate using a DVS (Intrinsic, Surface Measurement Systems, UK), at 35 °C, under a flow of $200 cm^3/min$ of nitrogen. An ultra-sensitive micro-balance allows measurement of sample mass variation as low as $0.1\,\mu g$. Nitrogen passes then through the chamber to maintain the desired relative humidity level.The accuracy on the air relative humidity is of $\pm$ 0.5 % and is of $\pm$ 0.1 °C on the temperature. A sample pan was designed in order to expose all faces of samples in chamber conditions. Approximately 95 mg of fresh sample, with an initial moisture content of ca. 13 kg/kg, dry basis, was inserted in the sample pan. Desorption tests were made from $a_w = 0.9$ to 0, by steps of 0.1. The criterium for equilibrium at each step was a mass rate less than 0.002 % per minute over a 15-min period. The parameters of the Guggenheim-Anderson-de Boer (GAB) model [17, 3, 8] were fitted to minimize the root mean square error (RMSE):

$$X_{eq} = \frac{X_{mono} c k a_w}{(1 - k a_w)\,(1 + (c-1) k a_w)} \quad (1)$$

Where X_{eq} is the equilibrium moisture content [kg/kg, d.b.]; X_{mono} is the monolayer moisture content [kg/kg, d.b.].; c is a parameter for sorption heat [-]; k is a constant [-], and a_w is the water activity [-].

GAB model was fitted to the curves by nonlinear regression, via Marquardt method, on the Statgraphics 19 Centurion software (Statgraphics Technologies, Inc., USA).

[Figure 1 about here.]

2.3. *Drying setup*

A magnetic suspension balance (10-µg-MSB, Rubotherm, Germany), with a resolution of 0.01 mg and a standard deviation of 0.02 mg [2], was used to follow the weight changes during drying. As the balance and the electromagnet are completely disconnected from the measuring chamber, high values of temperature and relative humidity can be tested without disturbance of the mass measurement (the balance and the upper part of the electromagnet are in the ambient environment, away from the hot airflow) and without cold points or leakage likely to perturb the conditions. Another advantage of this balance is that it can tare during the test, then preventing balance drift. The sample is attached to a hook (Fig. 1b), which is mounted on the permanent magnet of the suspension device. Compared to Almeida et al. [2], a new chamber was designed and realized to better meet the needs of this work. The changes in the oven also increased the observation area, allowing for the use of larger samples in comparison to previous work (Fig. 2a). In order to ensure isothermal conditions, the main body, of parallelepiped shape (35 mm (l) × 35 mm (w) ×100 mm (h)), is made of thick brass plates, an alloy with very good thermal conductivity, close to that of aluminum, suitable for precision machining and likely to resist corrosion from water flow for this device designed to work up to 90°C. The image acquisition system was designed in such way that the sample images can be grabbed during the test without perturbation of the weighting system, RH and temperature regulation. To meet this requirement, two windows (22 mm (l) × 47 mm (h)) are positioned on two opposite sides of the oven. These windows are double-walled to avoid condensation. Polished quartz was used for these windows because of its good optical properties. This permits the sample to be observed by shadowgraphy. We use two telecentric lenses, one for the lighting and one with the camera, to avoid any optical bias in the size

determination (camera: Pilot piA1600-35 gm, Basler, Germany; telecentric illumination: TECHSPEC 62-760, Edmund Optics Inc., USA and lens: VICOTAR T151/0.44, Vision and Control, Germany).

This device can control the temperature level in the range of 5 to 95 ° C. The relative humidity (RH) ranges from 0 to 98 % (accuracy of ±0.6 % at 23 ±5 °C). The new chamber performs robustly, with a peak to peak temperature variation equal to ±0.15 °C. The relative humidity is obtained by a moist air generator MHG-32, ProUmid GmbH and Co., Germany with a working range from 2 % to 98 % (accuracy of ± 0.6 % RH at 23 °C at ± 5 °C, 500 mL/min). We used two independent probes: one for the regulation and one to check and register the actual conditions. Both probes are placed upstream close to the sample to avoid the perturbation due to drying. Dry air (0 % RH) is achieved by using a three-way valve that shifts the inlet airflow from the humidity generator and dry nitrogen.

2.4. Drying protocol

The temperature and relative humidity of each experiment were defined as a central composite design [25]. The full experimental design is shown in Fig. 2b. The samples were dried between 5 and 7 h, depending on the drying conditions, until equilibrium was approached (dm/dt lower than 0.02 mg/min). During drying, the sample mass was collected every 30 s, and an image of the sample was taken every 180 s. At the end of each experiment, the sample was placed in an oven (at 70 °C, under <90 mmHg vacuum) for 24 h to determine its oven-dry mass.

The resolution of the raw projection images was 1600×1200 pixels. The deformation during drying was determined by digital image correlation (DIC), assuming a uniform deformation over the entire sample [27, 1].Therefore, 6 independent parameters were determined by DIC: one rotation angle, two translations (x and y) and three components of the deformation tensor (x and y deformation plus the shear angle). Out of these 6 parameters, only 2 are useful (deformation along x and y) while the shear deformation is just used to check the quality of the experiment (it must remain small). This treatment was done automatically over the full image series of each test using the in-house software *MeshPore* [26]. The algorithm implemented in *MeshPore* uses a formulation in large deformation, whose parameters are identified using the Simplex algorithm [35]. More details can be found in [27, 2].

[Figure 2 about here.]

2.5. Data analysis

The moisture content along the drying process was defined on dry basis as:

$$X = \frac{m(t) - m_s}{m_s} \tag{2}$$

where X is the moisture content $[kg.kg^{-1}d.b]$, $m(t)$ is the sample mass at a given time $[kg]$, and m_s is the oven-dry mass of the sample $[kg]$.

The directional deformations obtained in *MeshPore* express the dimensionless changes of length over the respective direction as a function of time, which is directly related to the global shrinkage coefficients of the sample:

$$\beta_L = \frac{h_0 - h(t)}{h_0} \quad ; \quad \beta_R = \frac{d_0 - d(t)}{d_0} \tag{3}$$

Where β_L and β_R are, respectively, the longitudinal and radial shrinkage coefficients [-]; h_0 and d_0 are, respectively, the initial height and diameter of the samples [m]; and $h(t)$ and $d(t)$ are, respectively, the height and diameter of the samples at time t [m].

To evaluate the differences between the shrinkage in the two directions, the anisotropy ratio, R_{ani}, is defined as the ratio between the radial and longitudinal shrinkage coefficients:

$$R_{ani} = \beta_R / \beta_L \tag{4}$$

In the case of a deformable product, the reduction of exchange surface area is likely to hinder the existence of a first drying stage period. The constant drying rate flux is revealed when accounting for the actual surface exchange area [24], and was subsequently proved by measuring the surface temperature, which remains at the wet bulb temperature during this period [29]. The global drying rate, Q_v $[kg.s^{-1}]$, as determined by the time-derivative of the sample mass, must therefore be analyzed in terms of drying rate per actual exchange surface area q_v $[kg.s^{-1}.m^{-2}]$:

$$Q_v = \frac{dm}{dt} = m_s \frac{dX}{dt} = A(t) q_v \tag{5}$$

where $A(t)$ is the actual area of exchange surface $[m^2]$.

To emphasize on the key point of the present work, the corrected rate is the sole rigorous concept for a deformable product. It will be noted q_v in the following. This is the drying rate flux $(kg.s^{-1}.m^{-2})$ per actual surface area $A(t)$. The uncorrected drying flux $q_{v,uncor}$

is the drying flux per initial surface area :

$$q_v(t) = \frac{1}{A(t)}\frac{dm}{dt} \tag{6}$$

$$q_{v,uncor}(t) = \frac{1}{A(t=0)}\frac{dm}{dt} \tag{7}$$

Assuming the sample to keep a cylindrical shape, which was observed for most of the drying process except at the very last stage, the actual surface area, which consists of the side face and both ends of the cylinder, reads as:

$$A(t) = \pi d(t)\left(\frac{d(t)}{2} + h(t)\right) \tag{8}$$

While the sample surface is supplied by free water, the sample temperature stabilized at the wet bulb temperature. In the case of highly deformable product, we get a period of constant drying flux (CDF), rather as the classical constant drying rate (CDR) period. As the sample temperature is constant during this period, the enthalpy balance is simple: the total heat supplied to the sample by convection, Q_h $[W]$ is used for phase change (liquid to water) of the water removed from the sample:

$$Q_v L_v = Q_h \tag{9}$$

Where L_v is the latent heat of vaporization $[J.kg^{-1}]$. The same relation can be derived in terms of fluxes per surface area:

$$q_v L_v = q_h \tag{10}$$

Where q_h is the heat flux per actual exchange surface area $[W.m^{-2}]$. During the CDF period, the drying flux q_v^0 is then simply determined by the heat transfer coefficient:

$$q_v^0 = \frac{h_h(T_s - T_w)}{L_v} \tag{11}$$

where h_h as the heat transfer coefficient $[Wm^{-2}.K^{-1}]$, T_s and T_w respectively as the dry-bulb and wet-bulb temperatures of the drying air (°C).

At the end of the CDF period, a function allows the decreasing drying rate stage to be represented, by a function of water content [24]:

$$q_v = q_v^0 F(X^*) \quad \text{where} \quad X^* = \frac{X - X_{eq}}{X_{cr} - X_{eq}} \tag{12}$$

In equation (12), X_{eq} is the equilibrium moisture content, as defined by the drying conditions and the sorption isotherms andX_{cr} is the critical moisture content, below which

the vapor pressure at surface becomes lower than the saturated vapor pressure. In the present work, the function F proposed by May and Perré [24] was used. This function has a continuous derivative at $X^* = 1$, which is consistent with the experiments, while parameter α defines the slope at $X^* = 0$:

$$F(X^*) = 1 \quad for X^* > 1$$
$$F(X^*) = \alpha X^* + (3 - 2\alpha)X^{*2} + (\alpha - 2)X^{*3} \quad for X^* \leqslant 1 \tag{13}$$

By working of our experimental data, we observed that the value of α must be as high as possible to match the experimental curves. This is why we always set $\alpha = 3$ as, above this value, the curve is not monotonic anymore (for $\alpha > 3$, $F"(1) > 0$).

2.5.1. Sample morphology during dehydration

Microscopic images of the samples were obtained using an environmental scanning electron microscope (ESEM, Quanta 200, FEI Company). Images were taken in environmental mode, at 667 Pa, voltage 13 kV, with a beam spot size of 4.5 and a working distance of approximately 8.5 mm. A sample of about 1 mm x 1 mm x 5 mm was inserted, using an in-house metallic sample support, designed to improve heat transfer from the Peltier stage to the sample. To observe saturated samples, the stage temperate was set at 2 °C, 667 Pa (RH = 95 %). Then, the stage temperature was increased to 10 °C, 667 Pa (RH 55 %) to observe the sample over time during the drying due to the decrease in relative humidity. The sampling process was similar to that described in Section 2.3. Samples were taken from the center of the root and observed in the transversal and longitudinal directions.

3. Experimental results

3.1. Vapor sorption isotherms

The vapor sorption isotherms, as depicted in Figure 3, are of Type III, which is common for solvent- and sugar-rich systems [5]. Shi et al. [41] studied the adsorption behavior of yacón and highlighted a sharp increase in the amount of adsorbed water at higher a_w, particularly for a_w value which exceeds 0.75. The same results were observed in the present work. Adjusting the GAB model, the parameters were $C = 0.559\,[-]$; $k = 1.00\,[-]$ and $X_{w,m} = 0.114\,[kg/kg\,d.b.]$, $R^2 = 0.9994$.

[Figure 3 about here.]

3.2. *Drying kinetics*

Table 1 presents the theoretical versus actual air conditions of all drying experiments. It can be observed that the experimental conditions previously defined are closely respected in the new chamber.

[Table 1 about here.]

In Fig. 4a, the experimental drying curve, along with the drying rates and selected corresponding images, are shown for one representative experimental test (60 °C, 20 % RH). One can see that the sample keeps the cylindrical shape, therefore enabling the estimation of its area by equation (8). The experimental determination of the sample size was used in the corrected rate shown in Fig. 4b. Note that the first and second drying periods are only visible when the drying rate curve is corrected by the actual exchange surface area of the sample (Fig. 4b). As already stated [24, 2], such an analysis is absolutely required to a rigorous assessment of the physical behavior. It requires the actual shape of the sample to be monitored continuously during drying, which is a major advantage of our experimental device. This correction is so accurate that we can even see the effect of the sample size on the heat transfer coefficient. As depicted in Fig. 4b), one can see that the drying rate flux slightly increases during drying, due to the reduction of the characteristic dimension. This effect is consistent with the dimensionless correlations [7, 47]. This effect was already observed, using a different method to obtained the *in-situ* and continuous deformation of potato [29]. With the chamber used in the present work, the heat transfer coefficient h_h, as computed using equation 12, increases from 19 to 21 $W.K^{-1}.m^{-2}$. This range is consistent with the values obtained using the same device with fiberboard samples for which shrinkage is negligible [32].

Note however that this treatment is no longer valid at the very last stages of drying (last image in Fig. 4a) as the sample ultimately loses its cylindrical shape. The characteristic drying curve, as computed with the fitted parameters of function$F$ is also plotted. One might note that the mathematical expression used has not enough degrees of freedom to perfectly fit the experimental values. Still, the trends are consistent and we believe it would not be relevant to add one degree of freedom for a slight improvement. The ultimate goal of this article is to propose a simple, but predictive model. If it were too complex, the approach would lose its operational value. Figure 4c depicts the drying rates obtained for a selected sub-set of experiments. The influence of temperature (50, 60, 70

°C) for the same relative humidity (20 %) condition is noticeable and seems to be more relevant in this case than the influence of different relative humidity values (10, 20, 30 %) maintaining the same temperature (60 °C). These trends are consistent with equation (11).

[Figure 4 about here.]

The results obtained for the full set of experiments are summarized in Table 2. The observed critical moisture content X_{cr} varies between 1.5 and 4.5 [g/g d.b.], with a considerable deviation between the repeated runs. The lowest value of X_{cr} was obtained at the highest drying temperature (70 °C), which can be explained by the thermal activation which eases the internal moisture migration and allows the deformation of the sample to occur without hardening. The drying air conditions have a clear influence on the initial drying rate, as shown in Fig. 5: the higher the difference between the drying air temperature and the wet-bulb temperature, the higher the initial drying rate, as expected from equation (11).

[Figure 5 about here.]

3.3. Shrinkage

In Table 2, Figs. 4a and 8b, it is noticeable that the longitudinal shrinkage is lower than the radial shrinkage. The calculated anisotropy ratio (radial/longitudinal shrinkage) was 1.64 ± 0.4 for the sample dried at 60 °C, 20 % RH. This ratio was defined at a moisture content of 3 kg/kg, db. This result is consistent those found in Marques et al. [23], in which convective drying of yacón slices were performed in a completely different experimental setup. In order to better understand the shrinkage of yacón, the cellular structure of saturated samples was observed by ESEM (Fig. 6). Figures 6a and b highlight two different types of cells: xylem vessels (presenting thick cell walls and a longitudinal orientation) and parenchyma cells (thin cell walls). Due to the high thickness of xylem vessels cell walls, they are likely to be less sensitive to collapse during drying, which would force collapse to occur mainly in radial direction. Note that the anisotropy factor could also be promoted at the final stages of drying by the adhesion of the sample to the support (Fig. 4a last image3). For this reason, shrinkage results in Table 2 were analyzed at a moisture content of 3 kg/kg (d.b.).

[Table 2 about here.]

[Figure 6 about here.]

The drying behavior of yacón roots at cellular level can be observed in the ESEM images (Fig. 7). Images 7a to 7d were taken from the same parenchyma cells and the collapse of these elliptical-shaped cells during drying becomes evident. It must be highlighted that the same method was applied to xylem vessels and it was not observed the collapse of these cells.

[Figure 7 about here.]

From the data on the central point repetitions (60 °C, 20 % RH), the yacón samples underwent a volume loss of 90.5 $\pm$ 0.1 %, after 6 h of drying. Other authors [38] reported an 89 % volume loss in yacón, dried first at 50 ° C for 5 h, then at 75 °C for another 5 h. It must be highlighted that the yacón variety used was not mentioned in the previous work, and is possibly a different variety than the one used in this work; also, the relative humidity was not reported. For potatoes, volume losses between 80 %[12] and 85 % [48] were reported; for apples, 72 % [15]; for bananas, 86% [10]; and for quince, 85 % [43]. The high initial water content and the observed cell collapse in yacón are factors that influence its considerable shrinkage. Potatoes, for example, have a lower water content; and apples form pores when drying [24, 2], resulting in a lower shrinkage than that observed in yacón.

It is interesting to note that the volume loss by the samples is consistently close to the volume of water loss for all drying conditions, as seen in Fig. 8. In the literature, similar results have been reported for yacón [38], potatoes [11, 24, 2] and pears [18]. This behavior can be explained by a full collapse of cells for a product with a very low initial porosity. This equivalence between loss of volume sample and volume of water removed will be called iso-volume deformation drying in the following. Note that, even for those products depicting iso-volume deformation, a deviation from the linear behavior was generally observed at the very last drying stage [2]. This is probably related to casehardening, once the absence of water can no longer act as a plasticizer for the cell wall.

For apples, a paper claims an iso-volume deformation [39], but other works, probably more reliable as they were performed with different experimental devices allowing continuous shape assessment, report a more pronounced volume reduction than water loss [24, 2]. This effect is attributed to the high initial porosity of apple: during drying, this porosity is likely to be reduced by the deformation of the cellular structure, which contributes to a higher reduction of the volume compared to the loss of water. A similar,

although less pronounced, effect was also observed for carrots [24]. For yacón, the similarity between volumetric water loss and the volume loss suggests that the initial porosity of this product is likely to be negligible.

[Figure 8 about here.]

4. The extended van Meel model

Contrary to comprehensive models of coupled heat and mass transfer [30, 28, 31], the van Meel [45] approach does not solve the internal heat and mass transfer inside the products. Instead, the physics of drying is embedded in the concept of Characteristic Drying Curve (CDC). This concept allows the drying rate at a certain averaged moisture content to be quantified as a function of the maximum drying rate, the so-called constant drying rate period (CDR). During this period, the water vapor pressure at the product surface remains equal to the saturated vapor pressure and the product temperature stabilizes at the web bulb temperature. The value of the CDR is then defined by equations (11) and (12). Beyond a certain value of moisture content, the critical moisture content X_{cr} introduced in section , the drying rate is just a fraction of this maximal drying rate and is defined by the function $F(X)$.

Rigorously, the value of X_{cr} and the shape of function F below X_{cr} depends on the drying conditions and on the product size. Contrary to comprehensive models, these dependencies cannot be predicted by the van Meel approach. Consequently, it remains valid and predictive as long as the drying conditions remain sufficiently close to the dataset used to define F and X_{cr}. This limitation is however counterbalanced by the simplicity of the model. In the initial paper published by Van Meel [45], the product is assumed to keep its initial shape throughout drying. In the case of yacón, concomitant facts allowed us to derive an extended van Meel model able to account for the shape reduction during drying:

1. An iso-volume deformation during a major part of the drying process,
2. The sample keeps a cylindrical shape over most of the drying process,
3. A very large initial moisture content, over 10 kg of water per kg of dry mass,
4. A low critical moisture content (1.5 to 4.5) compared to the initial moisture content (9.70 to 14.56 kg/kg, d.b.).

Fact 1 is the most important for the extended van Meel model: it allows the change of sample volume to be easily deduced from the drying rate. In addition, fact 2, together with the anisotropy ratio, allows the exchange surface area, to be predicted from the volume change, hence from the moisture content change. Hence, no shape measurement is needed to calculate the exchange surface area, a key quantity to obtain the drying rate.

Finally, facts 3 and 4, are a plus for the predictive ability of the model. As the dimensionless moisture content X^* is over than one for most part of drying, the value of function F is equal to 1 also for most part of the process and does not depend on parameter. The extended van Meel model is derived by combining equations 5, 8, 11 and 12. First of all, the volume variation is related to the drying rate, assuming an iso-volume deformation:

$$\frac{dV(t)}{dt} = \frac{1}{\rho_\ell}\frac{dm(t))}{dt} = -q_v^0\, A\,(t)\, F\,(X^*) \tag{14}$$

In equation (14), ρ_ℓ is the density of liquid water $[kg.m^{-3}]$ and q_v^0 is the drying rate flux $[kg.s^{-1}.m^{-2}]$ during the constant drying stage, as defined by equation (11).

In order to obtain a predictive model, the actual area of surface exchange $A(t)$ needs be computed over time. In the case of an isotropic product, $R_{ani} = 1$, the iso-volume deformation allows the evolution of radius and height to be simply derived from the volume change:

$$\frac{r\,(t)}{r_0} = \frac{h\,(t)}{h_0} = \left(\frac{V\,(t)}{V_0}\right)^{1/3} \tag{15}$$

In case of an anisotropic medium, we have to come back to the definition of directional shrinkage coefficients (equ. 4) to derive the values of $r(t)$ and $h(t)$ as a function of $V(t)$:

$$\frac{h\,(t)}{h_0} = 1 - \beta_L \quad ; \quad \frac{r\,(t)}{r_0} = 1 - \beta_R \tag{16}$$

Using the definition of the anisotropy ratio, we obtain a set of two decoupled equation to obtain β_L and β_R, hence $h(t)$ and $(d(t))$:

$$\frac{V(t)}{V_0} = (1 - \beta_L R_{ani})^2 \times (1 - \beta_L) \tag{17}$$

$$\beta_R = \beta_L R_{ani} \tag{18}$$

The equation (17) is a nonlinear equation that we simply solved using a Newton iteration method, which converges in 2 or 3 iterations.

Finally, the step-wise algorithm allowing the drying kinetics, as well as the shape evolution, to be computed reads as follows:

Algorithm 1: The extended van Meel algorithm

Initialization : set values of $h, d_0, h_0, \rho_s, X_{ini}, \alpha, X_{cr}, dt$;

$t \longleftarrow 0$;

while $t < t_{max}$ **do**

  Compute $q_v^0(t)$ using equ. (8) and actual conditions ($T_s(t)$ and $T_w(t)$);

  Compute dm and dV using equ. (16) and (11) ;

  $V(t+dt) \longleftarrow V(t) + dV$;

  $X(t+dt) \longleftarrow X(t) + dm/m_s$;

  if $R_{ani} = 1$ **then**

    Compute $h(t+dt)$ and $d(t+dt)$ using equ. (15);

  else

    Solve equ. (17) to obtain $\beta_L(t+dt)$;

    Compute $h(t+dt)$ and $d(t+dt)$ using equ. (18) and (16);

  end

  Update $A(t+dt)$ using equ. (8);

  Save data ;

  $t \longleftarrow t + dt$;

end

This algorithm is very simple to implement. In this work, a simple explicit Newton scheme, together with the solution of equation (17) was coded as a R script. The convergence was checked to be secured with a time step of 30 seconds.

The simulation results are depicted in figure 9 for the same test as presented in figure 4 ($T = 60\,°C; RH = 20\%$). The model kinetics (red solid line in fig. 9a) was computed with rounded values of the parameters obtained from the experiment ($h_h = 20\,W.K^{-1}.m^{-2}$, $R_{ani} = 2$, $\alpha = 3$, $X_{cr} = 3$). The prediction is in excellent agreement with the experimental data. In particular, one can see that the non-linear kinetics during the constant drying flux period, physically explained by the reduction of exchange surface area, is very nicely reproduced without any shape measurement. The Root Mean Square Error (RMSE) is equal to 13 % of moisture content. Keeping in mind that the initial moisture content equals 1400 %, this represents an excellent accuracy. The corrected and uncorrected drying rates are compared to the experimental ones in figure 9b. A slight difference between the predicted and the experimental curves can be observed during the falling drying rate period. However, we must keep in mind that i)we have here to deal with the derivative of experimental

data and ii) the computed curve is plotted as a function of the predicted moisture content, which increases the error.

To further emphasize the predictive ability of this model, two other simulations were performed to test its robustness. They are intended to quantify the error that would be done with a less documented behavior of the product:

- simulation assuming an isotropic shrinkage ($R_{ani} = 1$), blue dot-dashed line,
- simulation with $X_{cr} = 2$, instead of 3, dark red dotted line.

[Figure 9 about here.]

A tiny deviation is observed for an isotropic product (RMSE = 17 %), but the trend is still excellent. In the case of a smaller value of X_{cr}, the fit is even better (RMSE =9.5 %), with an excellent prediction of the moisture content at the end of drying. This is explained by the increase of the heat transfer coefficient as the sample reduces in size, which is attested by dimensionless correlations [7] and observed experimentally on samples of similar size [29]. For the sake of simplicity, this effect was not included in the present model and is partly compensated by a smaller value of X_{cr}, which delays the falling drying rate period. As the anisotropy ratio has little effect of the drying kinetics, this simple model relies on two main parameters:

- h_h defined by the flow configuration and which defines the constant drying flux, together with the dry and wet bulb temperatures,
- the critical moisture content X_{cr} which summarizes the product behavior

5. Discussion

Thanks to a device built around a magnetic suspension balance and using a new chamber specifically designed and manufactured for the present study, high quality and original data were collected during convective drying of yacón. These data allowed the drying of yacón to be carefully analyzed. In a first step, by correcting the drying rate by the real surface, a first very long drying period was highlighted. Regarding this fact, yacón behavior is very similar to that of potato [11, 24, 2]. Yet, in the case yacón, this behavior stands over a much wider range of moisture content : with an initial moisture content over 10 (dry basis), the first drying period last until a moisture content of 2 to 4 (dry basis). This

means that, for most of the drying time, the sample remains at the wet bulb temperature. This is of crucial importance to control the quality of the final product.

In addition, the analysis of sample volume tells us that yacón clearly depicts an iso-volume behavior. This means that the volume reduction equals the volume of remove water. This allows us to propose an extended van Meel model. Starting with the initial shape, the drying rate computed by the model is able to predict the reduction of sample volume. The model is therefore able to account for shrinkage in a predictive way. About 80% of the drying kinetics is then predicted with accuracy using one single parameters, the heat transfer coefficient, a parameter controlled solely by the chamber and the sample shape. In a production plant, all these features remains the same. In spite of the range of drying conditions tested, the observed range of critical moisture content remains quite narrow regarding the total amount of water to be removed. This is another observation that strengthens the predictive capacity of the model. This opens new control possibilities, for example by changing the drying conditions (temperature and relative humidity) over time as a function of energy availability or energy cost.

Therefore, this model accumulates many advantages : ease of implementation, low numbers of parameters, prediction ability and robustness. Coming back to the aim of this paper, i.e. to help the design of adapted drying strategies likely to preserve the nutritional quality of yacón, it is important to mention that the concept of characteristic drying curve as proposed by van Meel allows the product temperature $T(t)$ to be evaluated during the process [9]. By neglecting the heat capacity of the product, we get:

$$T(t) = T_d(t) - F(X^*)(T_d(t) - T_w(t)) \tag{19}$$

In an active control loop able to save energy and/or to reduce the energy cost, a criterion based on product quality by its temperature over time, can then be implemented.

6. Conclusion

In this paper, the convective drying of yacón was investigated using an in-house device which allows moisture content and sample dimensions to be continuously monitored under controlled conditions (temperature and relative humidity). The drying rate was corrected by the actual area of exchange surface. This rigorous analyze reveals two drying phases:

1. A constant drying flux period (sample temperature equals to the wet bulb temperature), which lasts during most part of drying, from the initial moisture content (ca. 13 kg/kg d.b.) to a critical moisture content ranging from 1.5 to 4.5 (kg/kg d.b.).
2. A decreasing drying flux period, which was represented by a suitable mathematical expression, defined by two parameters (X_{cr} and the initial slope).

The radial shrinkage was consistently more pronounced than the longitudinal one. Further investigation using environmental scanning electron microscopy (ESEM) showed that, for our samples collected in the central axis of the root, collapse occurs preferentially in radial direction, because the longitudinal direction is reinforced by thick cell wall vessels. For all drying conditions, we observed an iso-volume deformation during most part of the drying process: the reduction of sample volume equals the volume of removed water. Based on this observation, we proposed an extended van Meel model able to consider the large deformation of yacón during drying. The whole process can be nicely reproduced with only two key parameters: the heat transfer coefficient, which depends on the dryer configuration and the critical moisture content, a parameter depending on the product, but which acts only at the end of drying.

This model has great potential for application to any fresh product, provided that it features iso-volume deformation.

Acknowledgment

This work was supported by Coordination for the Improvement of Higher Education Personnel - Brazil CAPES- Finance Code 001; National Council for Scientific and Technological Development (CNPq), under Grant 309548/2021; and São Paulo Research Foundation (FAPESP), under Grants 2018/21327-1 and 2019/21832-0. Patrick Perré would like to thank the Département de la Marne, Greater Reims, Région Grand Est and the European Union along with the European Regional Development Fund (ERDF Champagne Ardenne 2014-2020) for their financial support of the Chair of Biotechnology of CentraleSupélec. The exchanges with Prof. María Victoria Coll Aráoz, from National University of Tucuman, Argentina, on yacón anatomy are also warmly acknowledged.

CRediT author statement

BM: Methodology, Formal analysis, Visualization, Writing-Original draft preparation, Writing–Reviewing and Editing. PP: Conceptualization, Methodology, Formal analysis, Mod-

eling, Visualization, Writing-Original draft preparation, Writing–Reviewing and Editing, Supervision, Funding acquisition. JC: Methodology, Writing-Reviewing and Editing. CT: Writing–Reviewing and Editing, Supervision, Funding acquisition. APF : Writing–Reviewing and Editing. GA: Conceptualization, Investigation, Methodology, ESEM images, Supervision, Writing-Original draft preparation, Writing-Reviewing and Editing.

Notations

The main notation are summarized in tables 3 and 4.

[Table 3 about here.]

[Table 4 about here.]

References

[1] G Almeida, F Huber, and P Perré. Free shrinkage of wood determined at the cellular level using an environmental scanning electron microscope. *Maderas. Ciencia y tecnología*, 16(2): 187–198, 2014.

[2] G Almeida, JP Lancha, F Pierre, J Casalinho, and P Perré. Physical behavior of highly deformable products during convective drying assessed by a new experimental device. *Drying Technology*, 35(8):906–917, 2017.

[3] Robert B Anderson. Modifications of the brunauer, emmett and teller equation1. *Journal of the American Chemical Society*, 68(4):686–691, 1946.

[4] FR Assis, LGG Rodrigues, G Tribuzi, PG De Souza, BAM Carciofi, and J. Laurindo. Fortified apple (malus spp., var. fuji) snacks by vacuum impregnation of calcium lactate and convective drying. *LWT*, 113:108298, 2019.

[5] S Basu, U. Shivhare, and AS Mujumdar. Models for sorption isotherms for foods: A review. *Drying technology*, 24(8):917–930, 2006.

[6] A Bernstein and CPZ Noreña. Study of thermodynamic, structural, and quality properties of yacon (smallanthus sonchifolius) during drying. *Food and Bioprocess Technology*, 7(1):148–160, 2014.

[7] RB Bird, WE Stewart, and Lightfoot EN. *Transport Phenomena*. John Wiley & Sons, New York, 1960.

[8] Jan Hendrik Boer et al. Dynamical character of adsorption. 1968.

[9] J Colin, R Rémond, and P Perré. Design and optimization of industrial woody biomass pretreatment addressed by DryKiln_CRP, a multiscale computational model: Particle, bed, and dryer levels. *Drying Technology*, 34(15):1820–1830, 2016.

[10] WP da Silva, I Hamawand, and Cleide MDPS e Silva. A liquid diffusion model to describe drying of whole bananas using boundary-fitted coordinates. *Journal of Food Engineering*, 137: 32–38, 2014.

[11] A Frias, G Clemente, and A Mulet. Potato shrinkage during hot air drying. *Food science and technology international*, 16(4):337–341, 2010.

[12] V Gekas and I Lamberg. Determination of diffusion coefficients in volume-changing systems—application in the case of potato drying. *Journal of Food Engineering*, 14(4):317–326, 1991.

[13] GR Gibson and MB Roberfroid. Dietary modulation of the human colonic microbiota: introducing the concept of prebiotics. *The Journal of nutrition*, 125(6):1401–1412, 1995.

[14] GR Gibson, ER Beatty, X Wang, and JH Cummings. Selective stimulation of bifidobacteria in the human colon by oligofructose and inulin. *Gastroenterology*, 108(4):975–982, 1995.

[15] R Golestani, A Raisi, and A Aroujalian. Mathematical modeling on air drying of apples considering shrinkage and variable diffusion coefficient. *Drying Technology*, 31(1):40–51, 2013.

[16] P Gorling. Physical phenomena during the drying of foodstuffs. *Fundamental Aspects of the Dehydration of Foodstuffs*, pages 42–53, 1958.

[17] EA Guggenheim. Applications of statistical mechanics, clarendon, 1966.

[18] R Guiné. Influence of drying method on density and porosity of pears. *Food and bioproducts processing*, 84(3):179–185, 2006.

[19] L Hassini, S Azzouz, R Peczalski, and A Belghith. Estimation of potato moisture diffusivity from convective drying kinetics with correction for shrinkage. *Journal of Food Engineering*, 79 (1):47–56, 2007.

[20] M Hermann. *Andean roots and tubers: ahipa, arracacha, maca and yacon*, volume 21. International Potato Center, 1997.

[21] M Hermann, I Freire, and C Pazos. Compositional diversity of the yacon storage root. *Impact on a changing world: Program report*, 98:425–432, 1997.

[22] JE Lozano, E Rotstein, and MJ Urbicain. Shrinkage, porosity and bulk density of foodstuffs at changing moisture contents. *Journal of food Science*, 48(5):1497–1502, 1983.

[23] BC Marques, A Plana-Fattori, D Flick, and CC Tadini. Convective drying of yacón (smallanthus sonchifolius) slices: A simple physical model including shrinkage. *LWT*, 159:113151, 2022.

[24] BK May and P Perré. The importance of considering exchange surface area reduction to exhibit a constant drying flux period in foodstuffs. *Journal of Food Engineering*, 54(4):271–282, 2002.

[25] DC Montgomery. *Design and analysis of experiments*. John wiley & sons, 2017.

[26] P Perré. MeshPore: a software able to apply image-based meshing techniques to anisotropic and heterogeneous porous media. *Drying technology*, 23(9-11):1993–2006, 2005.

[27] P Perré and F Huber. Measurement of free shrinkage at the tissue level using an optical microscope with an immersion objective: results obtained for douglas fir (pseudotsuga menziesii) and spruce (picea abies). *Annals of forest science*, 64(3):255–265, 2007.

[28] P Perré and BK May. A numerical drying model that accounts for the coupling between transfers and solid mechanics. case of highly deformable products. *Drying Technology*, 19(8): 1629–1643, 2001.

[29] P Perré and BK May. The existence of a first drying stage for potato proved by two independent methods. *Journal of food engineering*, 78(4):1134–1140, 2007.

[30] P Perré and IW Turner. A 3-D version of TransPore: a comprehensive heat and mass transfer computational model for simulating the drying of porous media. *International Journal of heat and mass transfer*, 42(24):4501–4521, 1999.

[31] P Perre, R Remond, and WI Turner. A comprehensive dual-scale wood torrefaction model: Application to the analysis of thermal run-away in industrial heat treatment processes. *International Journal of Heat and Mass Transfer*, 64:838–849, 2013.

[32] Patrick Perré, Romain Rémond, and Giana Almeida. Multiscale analysis of water vapor diffusion in low density fiberboard: Implications as a building material. *Construction and Building Materials*, 329:127047, 2022.

[33] CA Perussello, VC Mariani, and F Masson, Maria Land de Castilhos. Determination of thermophysical properties of yacon (smallanthus sonchifolius) to be used in a finite element simulation. *International Journal of Heat and Mass Transfer*, 67:1163–1169, 2013.

[34] CA Perussello, C Kumar, F de Castilhos, and MA Karim. Heat and mass transfer modeling of the osmo-convective drying of yacon roots (smallanthus sonchifolius). *Applied Thermal Engineering*, 63(1):23–32, 2014.

[35] WH Press, SA Teukolsky, WT Vetterling, and BP Flannery. *Numerical recipes in FORTRAN: The art of scientific computing*. Cambridge University Press, New York, 1992.

[36] C Ratti. Shrinkage during drying of foodstuffs. *Journal of food engineering*, 23(1):91–105, 1994.

[37] D Rocha, P de Ribeiro, A Caldas, B da Silva, A da Silva, A de Almeida, N da Silva, AM Machado, and R Alfenas. Acute consumption of yacon shake did not affect glycemic response in euglycemic, normal weight, healthy adults. *Journal of Functional Foods*, 44:58–64, 2018.

[38] CF Scher, A de Oliveira Rios, and CPZ Noreña. Hot air drying of yacon (smallanthus sonchifolius) and its effect on sugar concentrations. *International journal of food science & technology*, 44(11):2169–2175, 2009.

[39] EL Schultz, MM Mazzuco, RAF Machado, A Bolzan, MB Quadri, and MGN Quadri. Effect of pre-treatments on drying, density and shrinkage of apple slices. *Journal of Food Engineering*, 78(3):1103–1110, 2007.

[40] Q Shi, Y Zheng, and Y Zhao. Optimization of combined heat pump and microwave drying of yacon (s mallanthus sonchifolius) using response surface methodology. *Journal of Food Processing and Preservation*, 38(5):2090–2098, 2014.

[41] Q Shi, Y Zheng, and Y Zhao. Thermal transition and state diagram of yacon dried by combined heat pump and microwave method. *Journal of Thermal Analysis and Calorimetry*, 119(1): 727–735, 2015.

[42] Punit Singh and Prabal Talukdar. Determination of shrinkage characteristics of cylindrical potato during convective drying using novel image processing technique. *Heat and Mass Transfer*, 56(4):1223–1235, 2020.

[43] D A Tzempelikos, D Mitrakos, AP Vouros, AV Bardakas, AE Filios, and DP Margaris. Numerical modeling of heat and mass transfer during convective drying of cylindrical quince slices. *Journal of Food Engineering*, 156:10–21, 2015.

[44] K Valentová, A Lebeda, I Doležalová, D Jirovskỳ, B Simonovska, I Vovk, P Kosina, N Gasmanová, M Dziechciarková, and Ji Ulrichová. The biological and chemical variability of yacon. *Journal of agricultural and food chemistry*, 54(4):1347–1352, 2006.

[45] DA Van Meel. Adiabatic convection batch drying with recirculation of air. *Chemical Engineering Science*, 9(1):36–44, 1958.

[46] B Watzl, S Girrbach, and M Roller. Inulin, oligofructose and immunomodulation. *British Journal of Nutrition*, 93(S1):S49–S55, 2005.

[47] James R Welty, Charles E Wicks, Gregory Rorrer, and Robert E Wilson. *Fundamentals of momentum, heat, and mass transfer*. John Wiley & Sons, 2009.

[48] H Yang and N Sakai. Shrinkage and mechanical characteristics of potato undergoing air convection drying. *Jpn. J. Food Eng.*, 2(2):67–71, 2001.

List of Figures

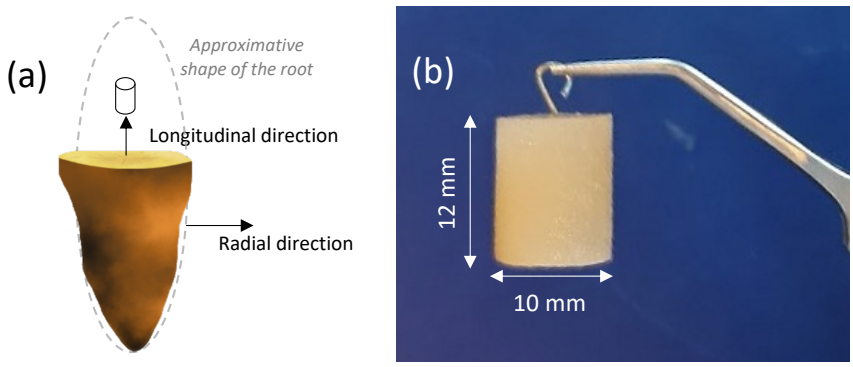

Figure 1: Sampling: (a) directions concerning the yacón root and (b) sample dimensions and metallic support.

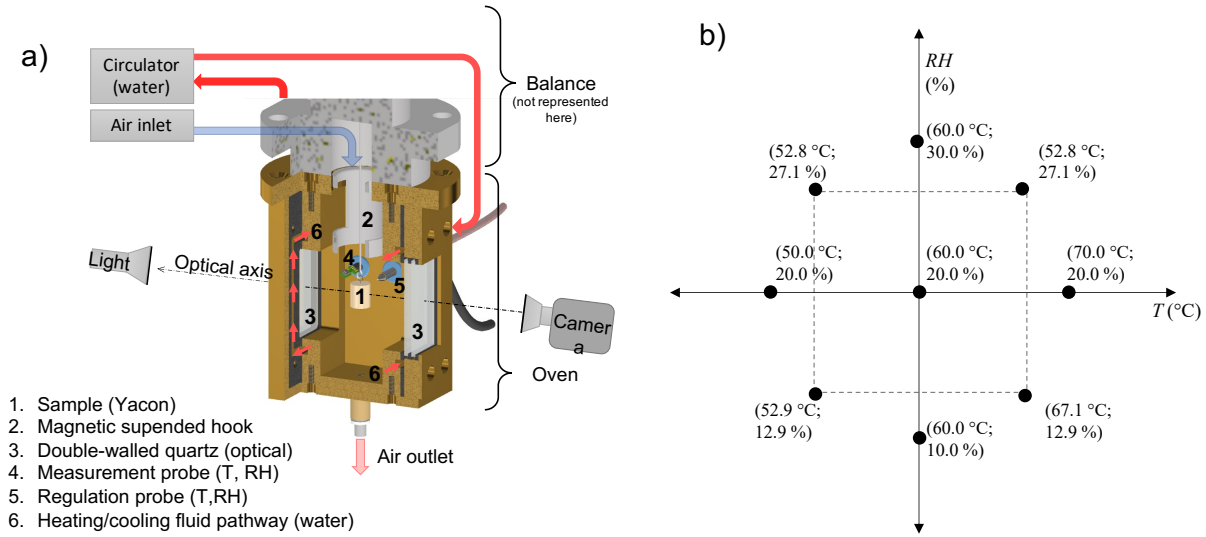

Figure 2: Drying protocol: (a) Schematic of the drying chamber with image grabbing and (b) Central composite experimental design.

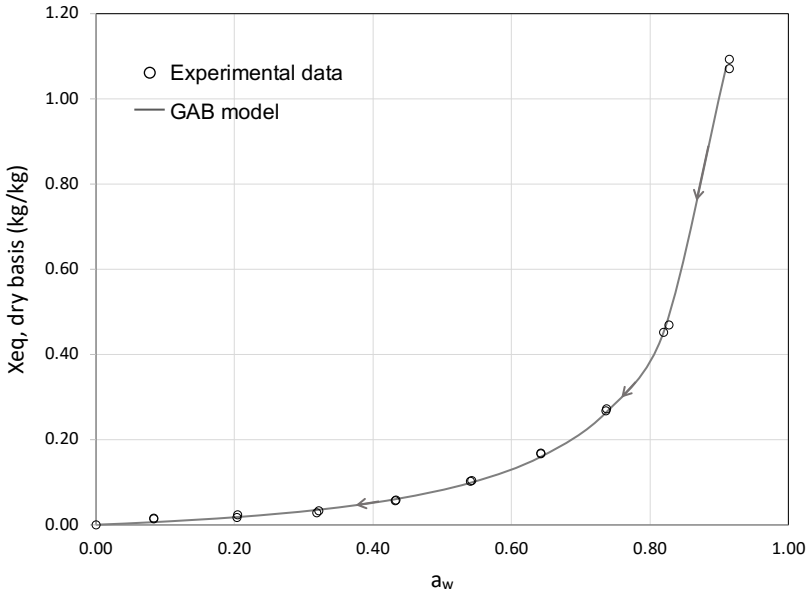

Figure 3: Vapor sorption isotherms of yacón samples obtained at 35 °C. Experimental values and adjusted GAB model.

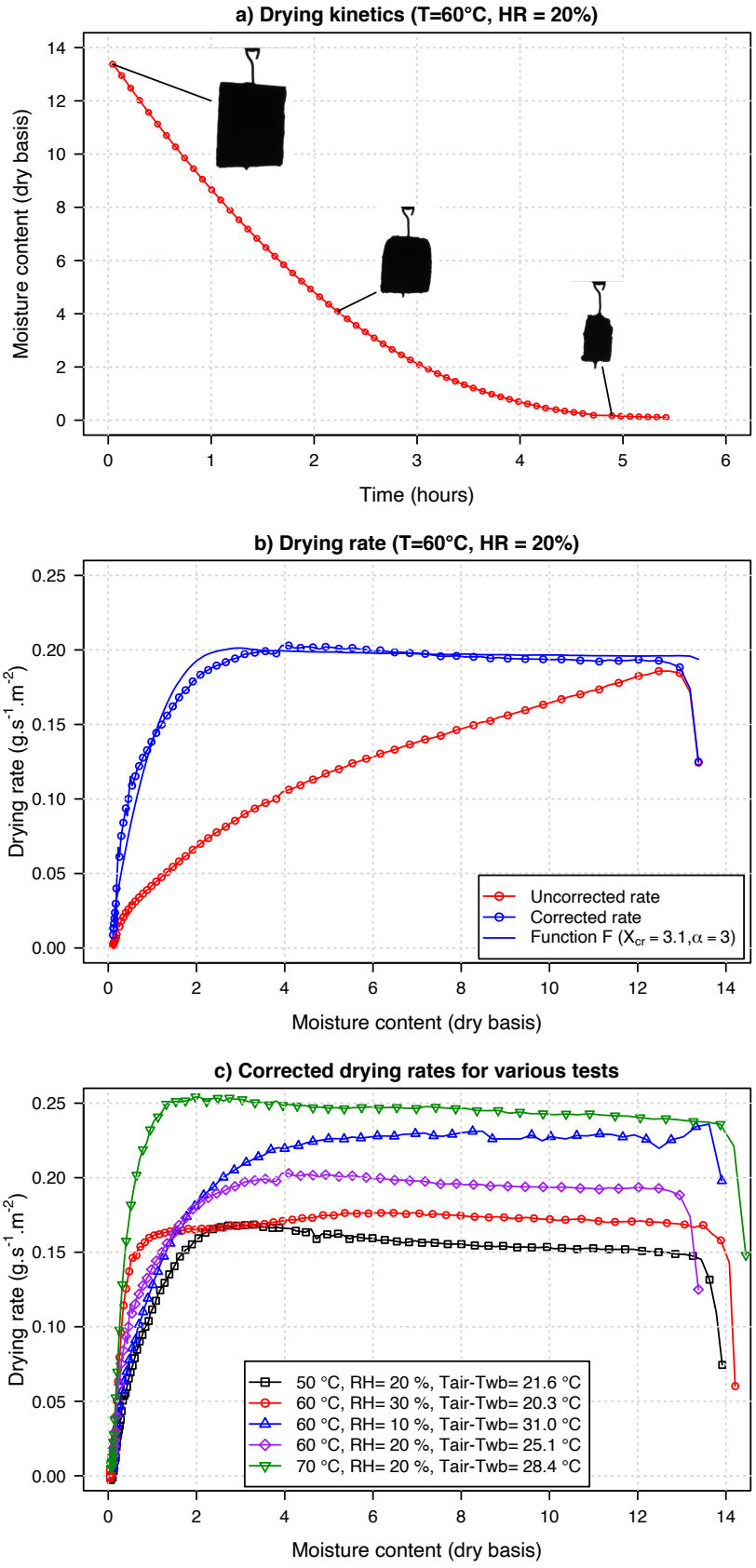

Figure 4: (a) Drying kinetics for an test performed at 60 °C, 20 % RH. Images of the sample at three contrasting times are inserted in this graph to illustrate the size reduction. (b) Drying rate versus moisture content, with and without correction by the actual surface area; (c) corrected drying rates of a subset of different drying conditions.

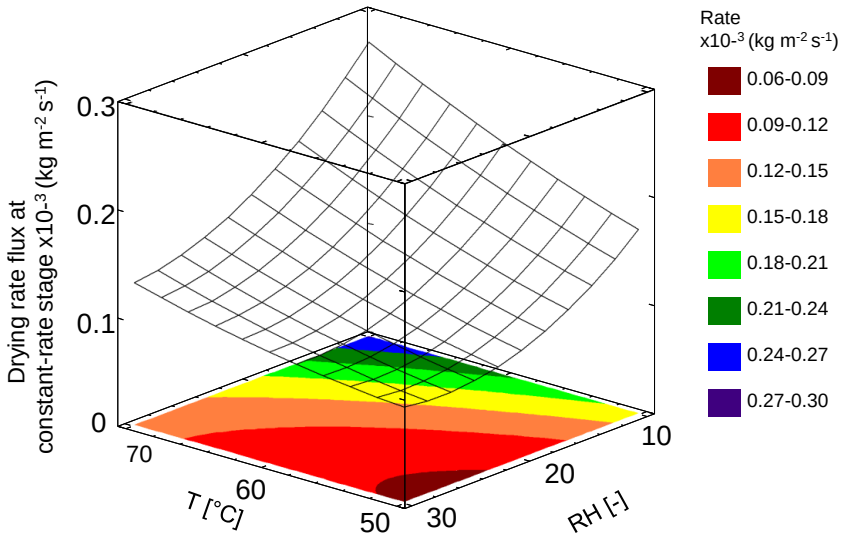

Figure 5: Response surface, showing the influence of the drying conditions on the initial drying rate.

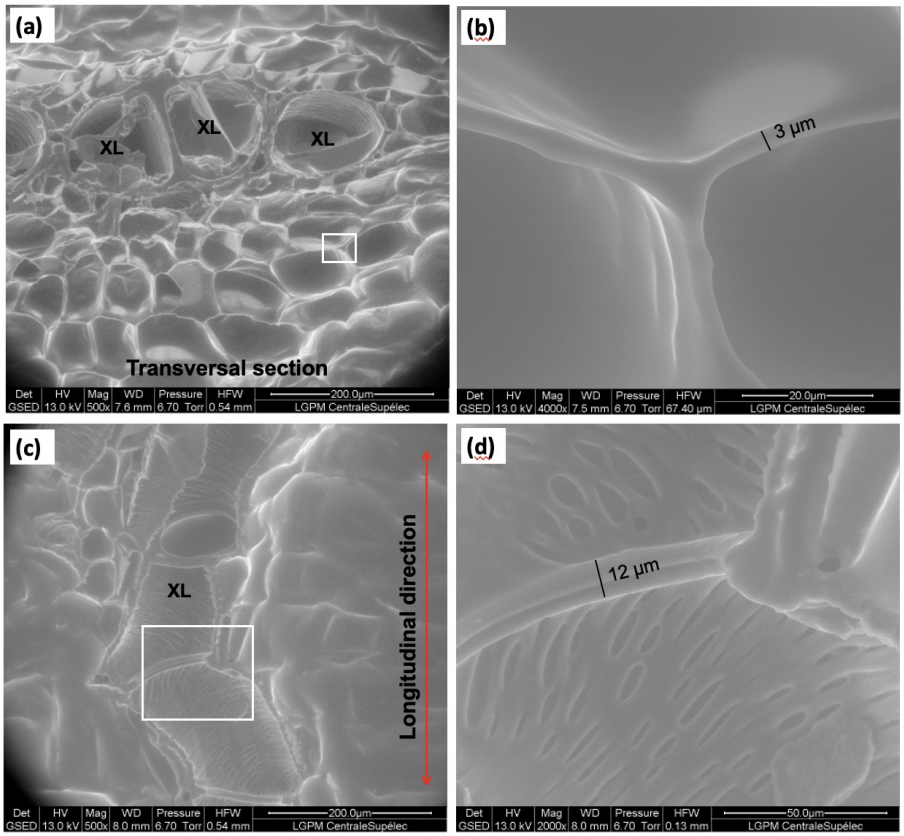

Figure 6: Images obtained by environmental scanning electron microscopy (ESEM) of yacón samples taken from the central axis of the root at saturating conditions (2 °C, P = 667 Pa, RH = 95 %). (a) Transversal section. (b) Increased magnification of the region marked with a white rectangle in "a". (c) Longitudinal section. (d) Increased magnification of the region marked with a white rectangle in "c". XL: xylem vessels.

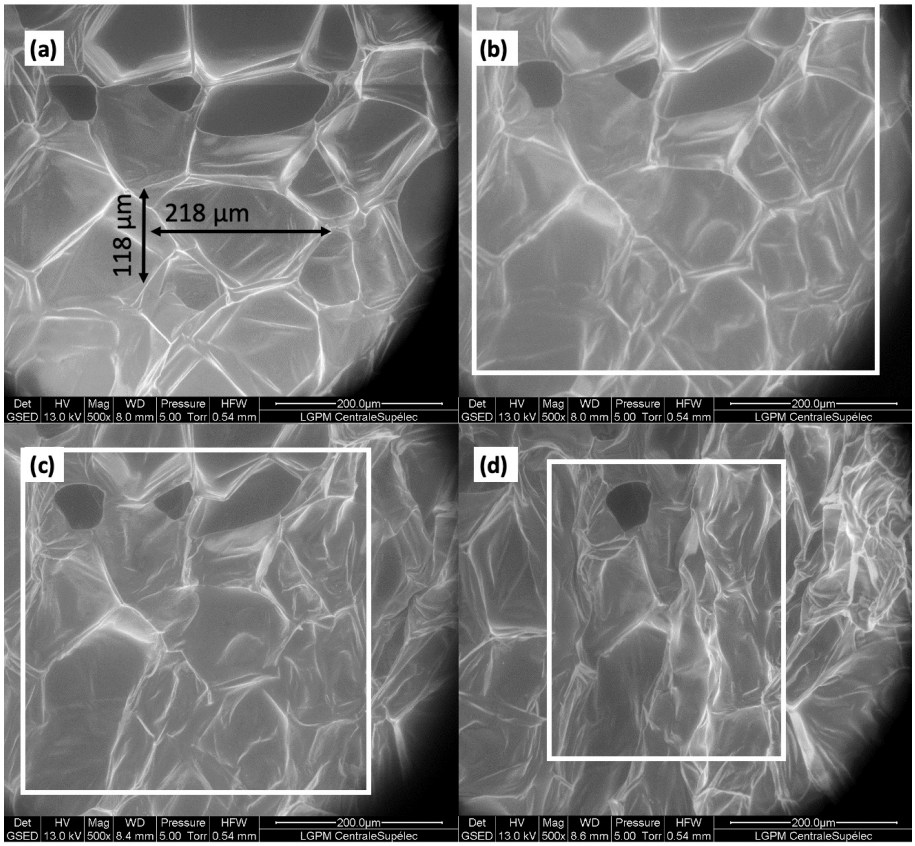

Figure 7: Images obtained by environmental scanning electron microscopy (ESEM) of yacón samples taken from the central axis of the root, transversal section (perpendicular to longitudinal section): (a) saturating conditions (2 °C, P = 667 Pa, RH = 95 %), (b) after 6 min of drying (10 °C, P = 667 Pa, RH ≈ 55 %); (c) after 10 min of drying (10 °C, P = 667 Pa, RH ≈ 55 %); (d) after 50 min of drying (10 °C, P = 667 Pa, RH ≈ 55 %) Rectangles indicate the shrinkage of the zone shown in (a).

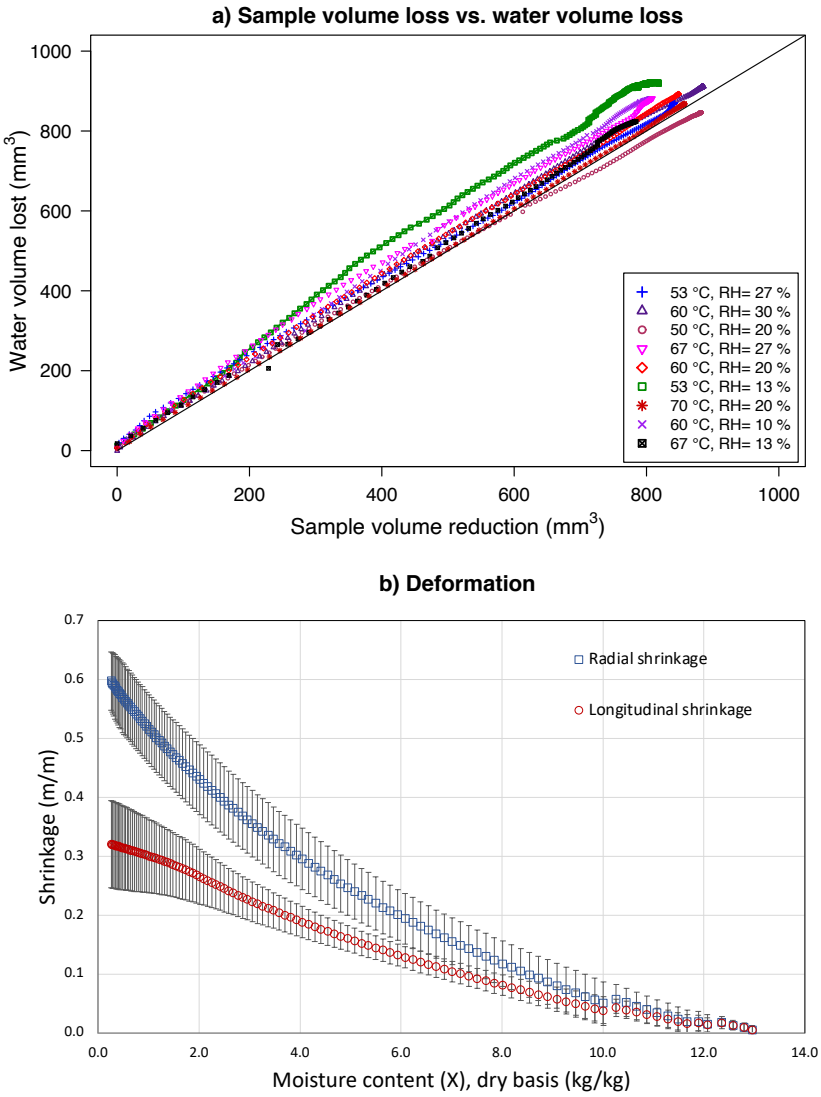

Figure 8: .(a) Sample volume loss vs. water volume loss by the yacón during the drying process, for all tested conditions, and (b) Change of dimension versus moisture content for samples dried at 60 °C, 20 % RH

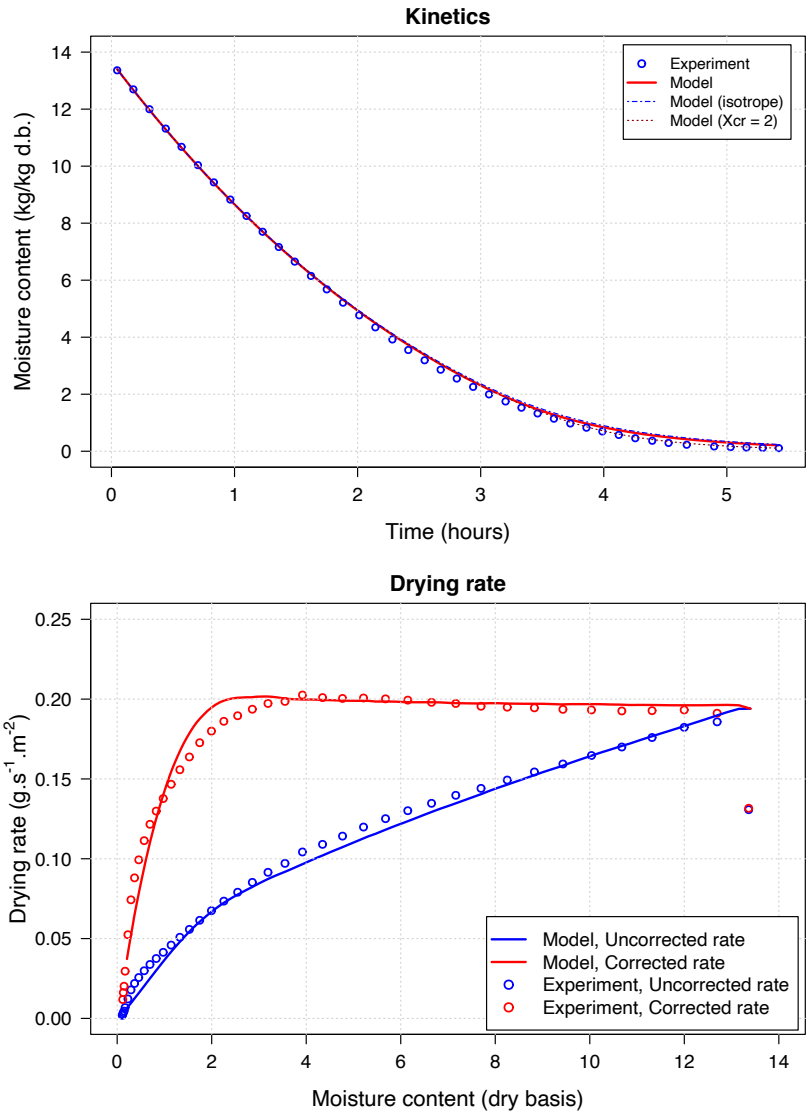

Figure 9: a) Kinetics simulation using the extended van Meel model. Experimental data from the ($T = 60\,^{\circ}C; RH = 20\%$) test. The model (red solid line) was computed with round values close to that obtained from the experiment ($h_h = 20\,W.K^{-1}.m^{-2}, R_{ani} = 2, \alpha = 3, X_{cr} = 3$). Simulations assuming an isotropic shrinkage ($R_{ani} = 1$) (blue dot-dashed line) and simulation with $X_{cr} = 2$, instead of 3 (dark red dotted line) are also proposed to prove the robustness of the model; b) Uncorrected and corrected drying rates curves predicted with the first set of parameters ($h_h = 20\,W.K^{-1}.m^{-2}, R_{ani} = 2, \alpha = 3, X_{cr} = 3$).

List of Tables

Table 1: Theoretical versus actual air conditions. The corresponding experimental wet bulb temperature and the difference between dry and wet bulb temperatures, are involved in equation 11, as also reported.

Test	T_{th} (°C)	RH_{th} (%)	T_{exp} (°C)	RH_{exp} (%)	$T_{w,real}$ (°C)	$T - T_{w,real}$ (°C)
1	52.8	12.9	53.67 ± 0.17	13.05 ± 1.27	27.26	26.41
2	52.8	27.1	53.38 ± 0.33	26.27 ± 0.86	33.47	19.91
3	67.1	12.9	67.59 ± 0.41	12.96 ± 0.66	35.00	32.59
4	67.1	27.1	67.30 ± 0.25	26.72 ± 0.36	43.78	23.52
5	60.0	20.0	59.97 ± 0.32	21.35 ± 0.58	35.62	24.34
6	60.0	20.0	60.17 ± 0.42	20.26 ± 0.69	35.03	25.14
7	60.0	20.0	60.50 ± 0.22	20.44 ± 0.56	35.62	24.88
8	60.0	20.0	60.29 ± 0.17	21.19 ± 0.68	35.54	24.76
9	60.0	20.0	60.31 ± 0.30	20.31 ± 0.57	35.19	25.13
10	70.0	20.0	69.93 ± 0.50	19.96 ± 0.43	41.67	28.24
11	50.0	20.0	51.45 ± 0.52	21.16 ± 0.91	29.76	21.69
12	60.0	30.0	60.31 ± 0.30	28.34 ± 0.73	39.49	20.82
13	60.0	10.0	59.81 ± 0.30	10.76 ± 1.07	28.99	30.82

Table 2: Summary of experimental conditions.

Test	T_{th} (°C)	RH_{th} (%)	$T_{w,th}$ (°C)	X_{cr} (-)	X_0 (-)	β_L (-)	β_R (-)	R_{ani} (-)
1	52.8	12.9	26.9	3.0	9.70	0.07	0.32	4.57
2	52.8	27.1	33.4	4.5	13.28	0.22	0.38	1.73
3	67.1	12.9	35.0	4.3	12.48	0.17	0.38	2.24
4	67.1	27.1	43.5	2.1	10.85	0.11	0.36	3.27
5 - 9*	60.0	20.0	34.9	3.3$\pm$0.7	11.95$\pm$1.5	0.23$\pm$0.03	0.36$\pm$0.06	1.64$\pm$0.40
10	70.0	20.0	41.6	1.6	14.56	0.25	0.42	1.68
11	50.0	20.0	28.4	2.1	13.97	0.20	0.43	2.15
12	60.0	30.0	39.7	4.3	14.20	0.23	0.41	1.78
13	60.0	10.0	29.0	4.2	14.11	0.20	0.38	1.90

* Tests 5 through 9 are repetitions of the central point.
β_L, β_R and R_{ani} were determined at 3 kg/kg, db.

Table 3: List symbols (Latin letters)

Symbol	Name	Unit
a_w	water activity	$-$
A	area of exchange surface	m^2
d	sample diameter	m
d_0	initial sample diameter	m
F	characteristic drying curve	$-$
h	sample height	m
h_0	initial sample height	m
h_h	heat transfer coefficient	$W.m^{-2}.K^{-1}$
Q_h	heat flux	W
q_h	heat flux density	$W.m^{-2}$
Q_v	vapor flux	$kg.s^{-1}$
q_v	vapor flux density	$kg.s^{-1}.m^{-2}$
L_v	latent heat of evaporation	$J.kg^{-1}$
m	mass	kg
m_s	dry mass	kg
RH	relative humidity	$-$ or $\%$
R_{ani}	anisotropy ratio	$-$
t	time	s
T	temperature	K or $°C$
T_d	dry bulb temperature	K or $°C$
T_w	wet bulb temperature	K or $°C$
V	sample volume	m^3
V_0	initial sample volume	m^3
X	moisture content, dry basis	$-$
X_{cr}	critical moisture content	$-$
X_{ini}	initial moisture content	$-$

Table 4: List of symbols (Greek letters)

Symbol	**Name**	**Unit**
α	parameter of the characteristic curve	$-$
β_L	longitudinal shrinkage	$-$
β_R	radial shrinkage	$-$
ρ_ℓ	liquid water density	$kg.m^{-3}$